ELSEVIER

International Journal of Heat and Fluid Flow 21 (2000) 489–498

International Journal of HEAT AND FLUID FLOW

www.elsevier.com/locate/ijhff

# DNS of turbulent flow along passively permeable walls

Claus Wagner [a,*], Rainer Friedrich [b]

[a] Institut für Strömungsmechanik, DLR Göttingen, Bunsenstr. 10, 37073 Göttingen, Germany
[b] Lehrstuhl für Fluidmechanik, TU München, Boltzmannstr. 15, 85748 Garching, Germany

**Abstract**

Fully developed low-Reynolds-number turbulent flow through straight permeable pipes with circular cross-section is investigated by means of direct numerical simulation. Three different cases of wall permeability are treated and compared with the case of a solid wall. In two of these cases, the wall satisfies the no-slip condition, but allows for the wall normal velocity fluctuations in two different ways. In the third case, the pipe wall has rectangular openings of size $(6\Delta z^+ \times 10(R\Delta\varphi)^+)$, regularly distributed over the whole surface, similar to a chessboard, where the white areas represent the openings and the black ones the solid wall. Velocity boundary conditions in the openings are such that the mean mass flux across the wall is zero and the flow in the openings is stress-free. All flows are driven by the same mean pressure gradient. Consequently, those flows which satisfy the no-slip condition have the same wall shear stress and hence the same turbulence Reynolds number $Re_\tau = 360$. Pipe flow with wall openings exhibits a small, but finite Reynolds shear stress at the wall. If the friction velocity is defined via the total stress at this wall, the flow nominally has the same turbulence Reynolds number. The overall effect of a permeable wall with rectangular openings is a mean axial slip velocity at the wall and reduced viscous stress. In a thin near-wall layer of thickness $\nu/u_\tau$, the turbulence activity is increased compared to the flow cases, where the velocity components satisfy the no-slip condition. All three rms-velocity fluctuations are non-zero. As a result the structure of the Reynolds stress tensor is modified in this region. This is also reflected in higher order central moments of the velocity fluctuations. A permeable wall with rectangular openings may be viewed as a model for a rough wall with a mean non-dimensional roughness height of 8.3 wall units. Close to such a wall the budgets of the Reynolds stress tensor differ strongly from those for flow along a smooth impermeable wall. 

*Keywords:* Pipe flow; Direct numerical simulation; Solid and permeable walls; Turbulence structure

## 1. Introduction

In recent direct numerical simulations (DNS), Wagner and Friedrich (1998a,b) have shown that turbulent flow through partially permeable pipes behaves similarly to flow through rough pipes. Wall permeability was modelled in such a way that the no-slip condition for the tangential components was retained, while the wall normal velocity was extrapolated from inner points and damped at a constant rate in accordance with the continuity condition. The analogy to flow through rough pipes was deduced from a comparison of mean velocity profiles with Nikuradse's log-law for rough pipes (Schlichting (1968)). The effective roughness heights obtained from this analogy varied from 15.5 to 19.8 wall units. Considerable changes in the turbulence structure were observed in the permeable wall cases as compared to the smooth solid wall case. They were documented in terms of rms-velocity fluctuations, Reynolds shear stress and flatness factors of the three velocity fluctuations. Two-point correlations of axial velocity fluctuations in the buffer layer indicated a slight reduction in the streak spacing, which is not obvious when instantaneous contour lines of axial velocity fluctuations are compared.

In the present investigation, we go a good step further and relax the no-slip constraint at the permeable wall assuming rectangular openings in the wall in which velocity fluctuations can develop freely in all three directions. This is achieved on the basis of stress-free boundary conditions and the continuity constrain. The pipe with openings can be imaged as being surrounded by a pipe of bigger diameter filled with the same fluid.

The paper comprises a discussion of the numerical method used to integrate the incompressible Navier–Stokes equations, the boundary conditions and computational parameters. Most of the results deal with a comparison of mean flow quantities for three different permeable walls and a solid wall. Changes in the turbulence structure resulting from the wall permeability are discussed in terms of second and higher order central moments of the velocity fluctuations and finally in terms of budgets of the four non-zero Reynolds stresses.

* Corresponding author. Tel.: +49-551-709-2261; fax: +49-551-709-2446.

*E-mail address:* claus.wagner@dlr.de (C. Wagner).

0142-727X/00/$ - see front matter 
PII: S0142-727X(00)00036-9

**Notation**

| | |
|---|---|
| $D$ | pipe diameter |
| $k$ | turbulent kinetic energy |
| $k_R$ | roughness parameter |
| $p$ | pressure |
| $r$ | radial coordinate |
| $R$ | pipe radius |
| $Re_\tau$ | Reynolds number based on $u_\tau, D$ |
| $Re_b$ | Reynolds number based on $U_b, D$ |
| $R_{u_z u_z}$ | two-point autocorrelation of axial velocity fluctuations |
| $\vec{u}$ | velocity vector |
| $u_z, u_\varphi, u_r$ | velocity components in axial, circumferential, radial direction |
| $u_\tau$ | friction velocity |
| $U_b$ | bulk velocity |
| $y = R - r$ | wall normal coordinate |
| $z$ | axial coordinate |

*Greeks*

| | |
|---|---|
| $\alpha$ | damping factor to control the radial velocity component at the wall; ranges from 0 (solid wall) to 1 (perfectly permeable wall) |
| $\lambda$ | friction factor, streak spacing |
| $\varphi$ | azimuthal coordinate |
| $\rho$ | density |
| $\nu$ | kinematic viscosity |

*Other symbols*

| | |
|---|---|
| $\langle..\rangle$ | Reynolds average |
| $(..)'$ | fluctuation |
| $\nabla$ | gradient |
| $\nabla^2$ | Laplacian |
| $\Delta$ | finite difference |
| $(..)^+$ | quantity non-dimensionalized by wall units, either $u_\tau$ or $\nu/u_\tau$ |

## 2. Numerical method and computational details

The Navier–Stokes equations for incompressible flow

$$\nabla \cdot \vec{u} = 0, \tag{1}$$

$$\frac{\partial \vec{u}}{\partial t} + \nabla \cdot (\vec{u}\vec{u}) = -\frac{1}{\rho}\nabla p + \nu \nabla^2 \vec{u}, \tag{2}$$

are integrated in a cylindrical $(z, \varphi, r)$-coordinate system using staggered grids and second-order central differencing. A semi-implicit time-integration scheme advances the solution in time. Only those convection and diffusion terms are treated implicitly, which contain derivatives in the circumferential direction. Thus, time step restrictions resulting from small grid spacing $r\Delta\varphi$ near the centreline are avoided. The remaining convection terms are advanced in time using the second-order accurate leap-frog scheme. The pressure gradient is split into a constant mean part, which drives the flow and a fluctuating part. The latter is neglected in the first sub-step of the projection method and then used to correct the velocity field. The 3D Poisson equation which provides the fluctuating pressure field is solved directly via FFT in the homogeneous $(z, \varphi)$-directions and a standard tridiagonal matrix algorithm.

### 2.1. Boundary conditions

The fluctuating pressure and instantaneous velocity vector are periodic in axial and circumferential directions.

At the wall, the fluctuating pressure satisfies a von Neumann condition, irrespective of whether the wall is solid or permeable. No-slip and impermeability conditions hold at the solid wall (DNS 1). In the two permeable wall cases, the no-slip conditions

$$u_z = u_\varphi = 0 \quad \text{at} \quad r = R \tag{3}$$

are satisfied, but the wall permeability for the radial velocity component is modelled as follows:

$$(u_r r)_{r=R} = \alpha (u_r r)_{r=R-\Delta r}. \tag{4}$$

In case of DNS 2, each cell along the wall is partially permeable, with $\alpha = 0.975$. In DNS 3, each second wall cell in $(z, \varphi)$-directions is either solid ($\alpha = 0$) or perfectly permeable ($\alpha = 1$). Finally, in DNS 4 the wall has rectangular openings, in which zero-stress conditions

$$\mu \left( \frac{\partial u_r}{\partial z} + \frac{\partial u_z}{\partial r} \right)_{r=R} = 0, \tag{5}$$

$$\mu \left( r \frac{\partial u_\varphi / r}{\partial r} + \frac{1}{r} \frac{\partial u_r}{\partial \varphi} \right)_{r=R} = 0, \tag{6}$$

are satisfied along with the continuity condition

$$\left( \frac{\partial u_z}{\partial z} + \frac{1}{r} \frac{\partial u_\varphi}{\partial \varphi} + \frac{1}{r} \frac{\partial r u_r}{\partial r} \right)_{r=R} = 0. \tag{7}$$

If the extrapolation of $u_r$ in (4) or (7) violates the mass balance, continuity is enforced. Consequently, the mean velocity component in radial direction must vanish.

### 2.2. Computational parameters

The domain in which the computations are performed is a pipe of diameter $D = 2R$ and length $5D$. It is resolved by an equidistant grid of $480 \times 240$ points in $(z, \varphi)$-directions, respectively. Along the radius ($R$), 70 points are non-equidistantly distributed, with the first point at $y^+ = 0.185$. The Reynolds number based on friction velocity, $u_\tau$, and diameter, $D$, is $Re_\tau = 360$. In wall units the grid spacing is

$$\Delta z^+ = 3.75,$$

$$(r^+ \Delta\varphi) = 0.073\text{–}4.71, \tag{8}$$

$$\Delta r^+ = 0.185\text{–}5.56.$$

The wall openings in the case of DNS 4 have the size $(1/8 \times \pi/20)R^2$ in $(z, \varphi)$-directions or $(22.5 \times 28.26)$ in wall units which correspond to $(10 \times 6)$ cells. They are arranged similarly to a chessboard as indicated in Fig. 1, where the white fields represent the openings.

In all simulations, the flow was observed and averaged over more than 10 eddy turnover times $D/u_\tau$ during which the bulk velocity remained stable. The computations were started from previous DNS of pipe flow along solid/permeable walls.

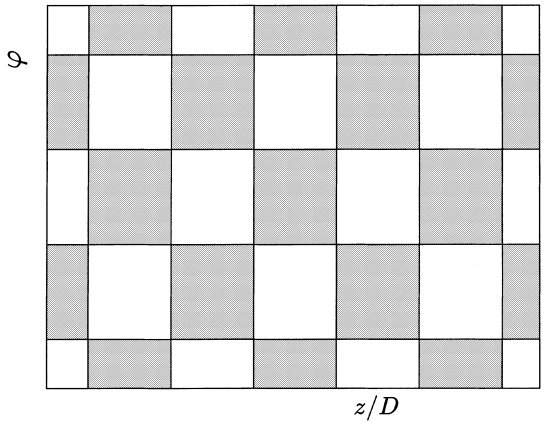


Fig. 1. Wall openings (white) of size $22 \times 28\nu^2/u_\tau^2$.

## 3. Results

### 3.1. Snapshot of instantaneous velocity field

The effect of the wall openings on the velocity field is demonstrated for DNS 4 in Fig. 2, where contours of the instantaneous streamwise velocity field are plotted in unrolled wall parallel surfaces for a wall distance of $y^+ = 2$. Close to the wall, $u_z$ reflects the chessboard-like structures, which are a result of the no-slip and stress-free conditions at the wall. Superimposed are streaky structures, which are generated in wall bounded shear flows by the up and down of slow and fast fluid (see Wagner and Friedrich (1998a)).

### 3.2. Mean flow field

We use triangular brackets to define statistical averages. Except for $\langle p \rangle$, they are obtained from DNS data by sampling in $z$- and $\varphi$-directions and in time. Table 1 presents an overview over the four direct simulations performed, including global flow parameters like $Re_\tau$, the Reynolds number $Re_b$, based on bulk velocity $U_b$ and the friction factor $\lambda$ defined by

$$\frac{\mathrm{d}\langle p \rangle}{\mathrm{d}z} = -\frac{\lambda}{D}\frac{\rho}{2}U_b^2. \tag{9}$$

A roughness height, $k_R$, underlining the similarity between flow through permeable and rough pipes, is computed, using Nikuradse's law for the rough pipe (Schlichting (1968))

Table 1
Parameters of fully developed turbulent flow in pipes with partially permeable walls (DNS 2,3,4) and a solid wall (DNS 1)

| DNS | 1 | 2 | 3 | 4 |
|---|---|---|---|---|
| $Re_\tau$ | 360 | 360 | 360 | 360 |
| $\alpha$ | 0.0 | 0.975 | – | – |
| $Re_b$ | 5317 | 4406 | 4691 | 5252 |
| $U_b/u_\tau$ | 14.77 | 12.24 | 13.03 | 14.59 |
| $\lambda \cdot 10^2$ | 3.67 | 5.30 | 4.71 | 3.76 |
| $k_R/D$ | – | 0.055 | 0.043 | 0.023 |
| $k_R^+$ | – | 19.8 | 15.5 | 8.28 |

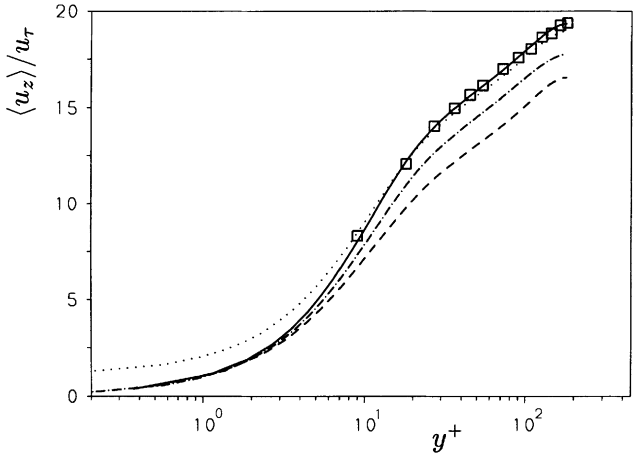


Fig. 3. Mean velocity profile in a solid and in permeable pipes. DNS 1: ——, DNS 2: – –, DNS 3: — · —, DNS 4: ·····, LDA measurements of Westerweel et al. (1992): □.

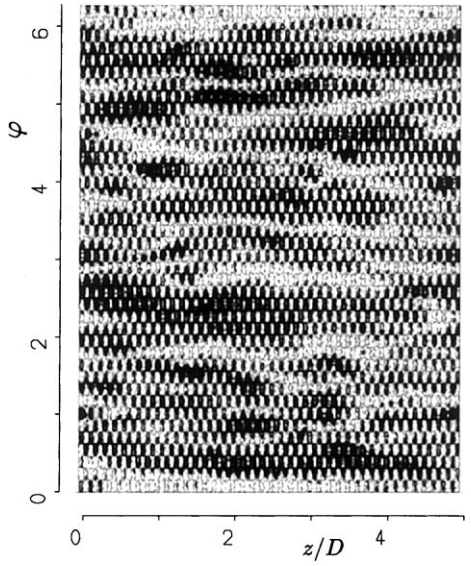


Fig. 2. Contours of streamwise velocity $u_z$ in wall parallel planes for a wall distance of $y^+ = 2$. Black/gray lines represent positive/negative values, respectively.

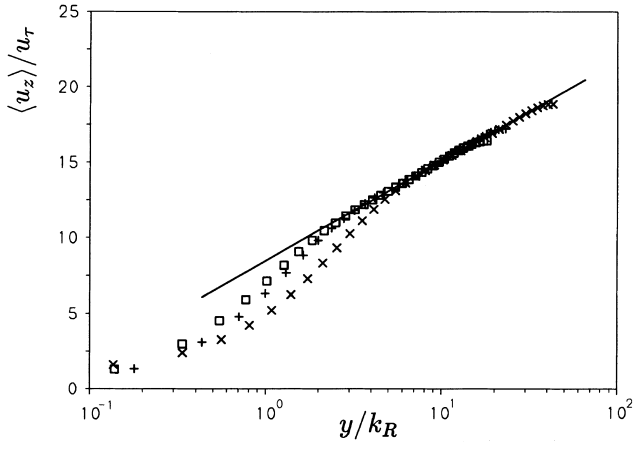


Fig. 4. Mean velocity profiles versus wall distance normalized with the roughness height. DNS 2: □, DNS 3: +, DNS 4: ×, Nikuradse's log-law: —— .

$$\frac{\langle u_z \rangle}{u_\tau} = 2.87 \ln\left(\frac{y}{k_R}\right) + 8.48, \tag{10}$$

with a slope modified from 2.5 to 2.87.

The numbers in Table 1 indicate that wall permeability reduces the flow rate through the pipe and increases the drag due to enhanced turbulence activity. Permeable walls act similarly to rough walls with roughness heights reaching the buffer layer of turbulent flow through a solid pipe.

The mean axial momentum transport in all flow cases is governed by the balance between pressure gradient, viscous and Reynolds shear stress

$$-\frac{r}{2}\frac{1}{\rho}\frac{\partial\langle p\rangle}{\partial z} + \nu\frac{\mathrm{d}\langle u_z\rangle}{\mathrm{d}r} - \langle u_z' u_r'\rangle = 0. \tag{11}$$

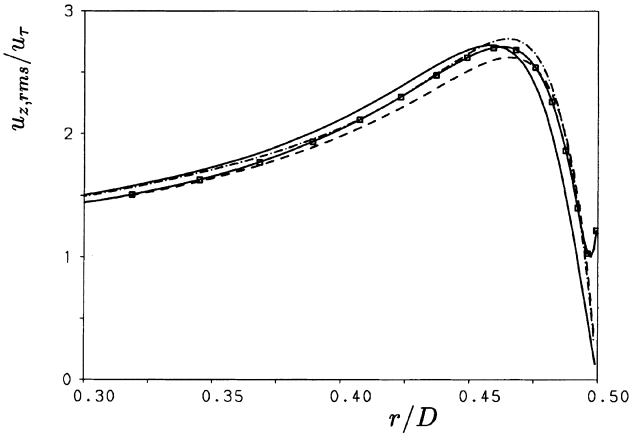


Fig. 5. Profiles of axial rms-velocity fluctuations for DNS 1: ——, DNS 2: - - - -, DNS 3: — · — · —·, and DNS 4: —□—.

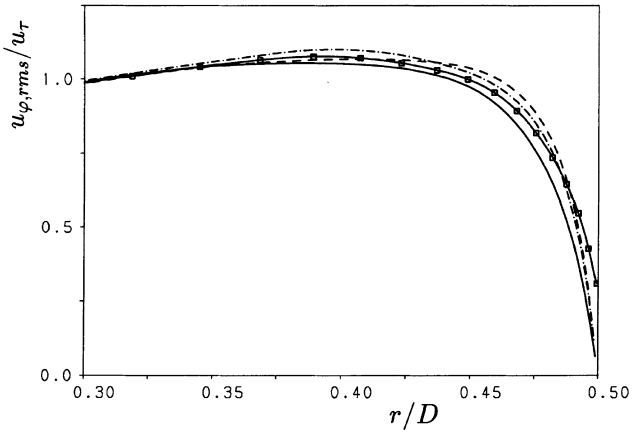


Fig. 6. Circumferential rms-velocity fluctuations. Lines as in Fig. 5.

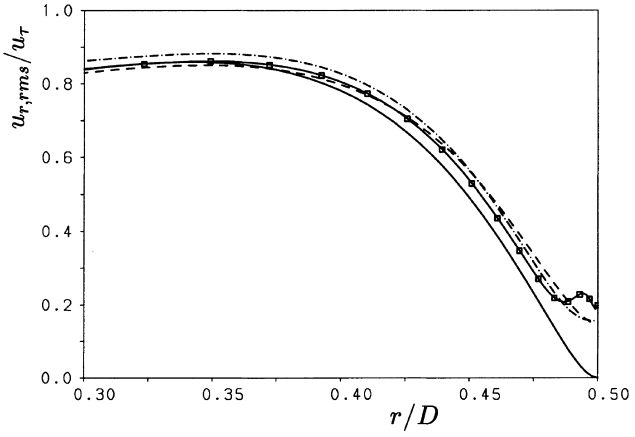


Fig. 7. Profiles of radial rms-velocity fluctuations. Lines as in Fig. 5.

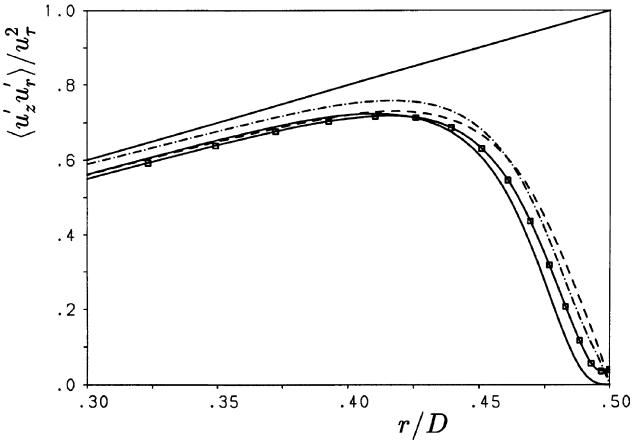


Fig. 8. Profiles of total and Reynolds shear stresses. Lines as in Fig. 5.

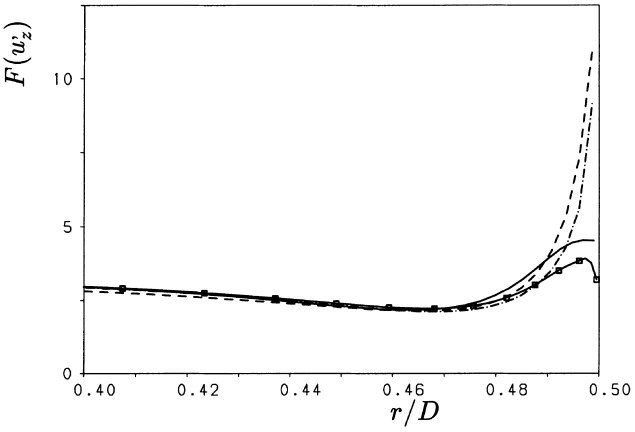


Fig. 9. Flatness factors of axial velocity fluctuations. Lines as in Fig. 5.

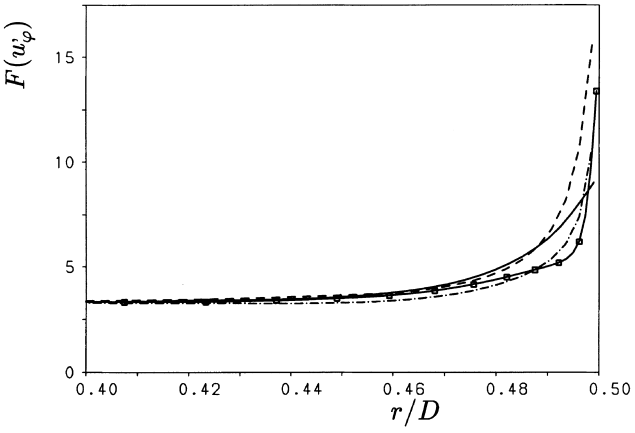


Fig. 10. Flatness factors of circumferential velocity fluctuations. Lines as in Fig. 5.

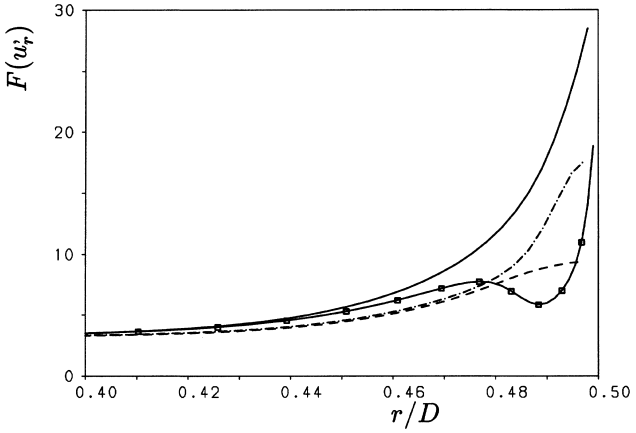


Fig. 11. Flatness factors of radial velocity fluctuations. Lines as in Fig. 5.

This equation already reflects the linearity of the total shear stress (sum of viscous and Reynolds stress). If in all flow cases the pressure gradient is used to define the friction velocity according to

$$\frac{\partial\langle p\rangle}{\partial z} = -\frac{2}{R}\rho u_\tau^2, \tag{12}$$

$$\frac{1}{Re_\tau}\frac{\mathrm{d}(\langle u_z\rangle/u_\tau)}{\mathrm{d}(y/D)} + \frac{\langle u_z' u_r'\rangle}{u_\tau^2} = 1 - 2\frac{y}{D}, \tag{13}$$

where the $y$-coordinate has been introduced as $y = R - r$. It is easy to show that Taylor expansions of $u_z^+ = \langle u_z\rangle/u_\tau$ near the wall, in terms of powers of the wall coordinate $y^+ = yu_\tau/\nu$, have the following forms:

*Solid wall (DNS 1)*:

$$u_z^+ = y^+ - \frac{1}{8}\left\langle \frac{\partial u_z^{+\prime}}{\partial y^+}\frac{\partial^2 u_r^{+\prime}}{\partial y^{+2}}\right\rangle_0 y^{+4} - \cdots \tag{14}$$

*Permeable wall with no-slip condition (DNS 2,3)*:

$$u_z^+ = y^+ - \left(\frac{2}{Re_\tau} + \left\langle \frac{\partial u_z^{+\prime}}{\partial y^+} u_r^{+\prime}\right\rangle\right)_0 \frac{y^{+2}}{2} - \cdots \tag{15}$$

*Permeable wall with stress-free openings (DNS 4)*:

$$u_z^+ = u_z^+(0) + (1 - \langle u_z^{+\prime} u_r^{+\prime}\rangle_0)y^+ - \left(\frac{2}{Re_\tau} + \frac{\mathrm{d}}{\mathrm{d}y}\langle u_z^{+\prime} u_r^{+\prime}\rangle\right)_0 \frac{y^{+2}}{2} - \cdots \tag{16}$$

Along a solid wall, a viscous sublayer of thickness $5\nu/u_\tau$ develops, in which the velocity profile is linear. The permeable wall with vanishing tangential velocity components experiences the full viscous stress, but due to the rapid near wall raise of the Reynolds shear stress there is no viscous sublayer. The velocity profile is parabolic close to the wall. At the permeable wall with openings, we observe in the mean a small, but finite slip velocity $u_z^+(0)$ and reduced viscous stress. Again, there is no viscous sublayer and a parabolic velocity profile close to the wall.

Fig. 3 shows mean velocity profiles in wall units for solid and permeable pipes. The solid wall data compare very well with LDA measurements of Westerweel et al. (1992) for the same Reynolds number. Permeable pipes generate profiles with a downward shift of the core layer part. This behaviour is also typical for flow through rough pipes. A 'first-order' similarity

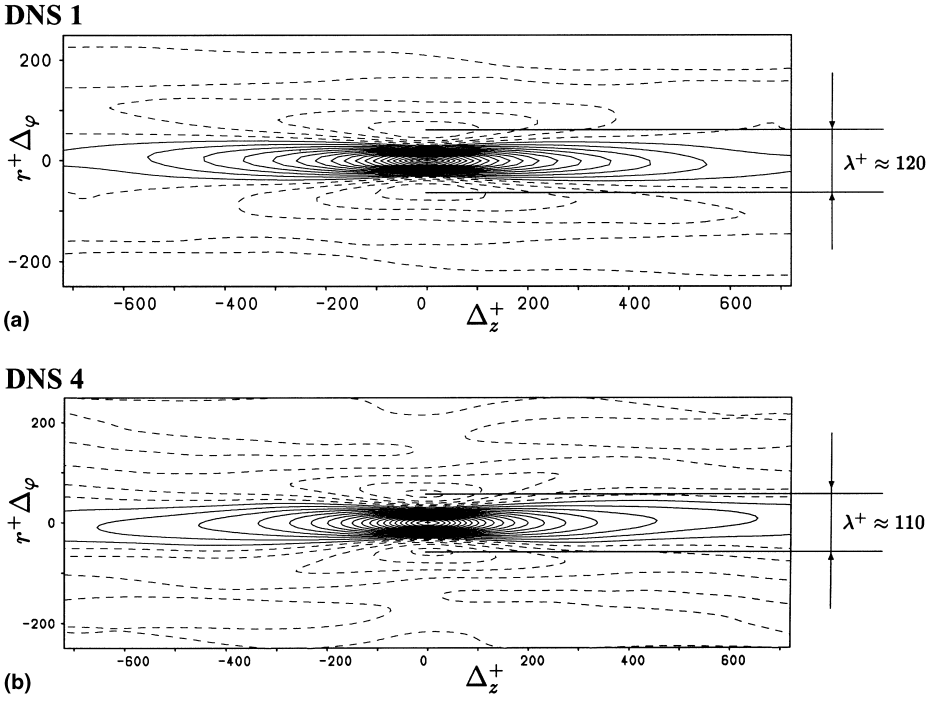


Fig. 12. Contour lines of the two-point correlation $R_{u_z u_z}$ defined in Eq. (17) in a pipe with solid walls (a) and a pipe with wall openings (b) for $Re_\tau = 360$.

between flow through permeable and rough pipes is obvious from Fig. 4, where the mean velocity is plotted against $y/k_R$. The law for the rough pipe, Eq. (10) is hence valid in the core region of any of the flows through permeable pipes. Further similarities have to be searched, based on the turbulence structure.

Table 2
Wall values of terms in the balance equations for $\langle u_z'^2\rangle$, $\langle u_\varphi'^2\rangle$, $\langle u_r'^2\rangle$. Zero/finite values are indicated by 0/*f*

| | P | D | PS | PD | TD | VD |
|---|---|---|---|---|---|---|
| DNS 1 | 0,0,0 | *f*,*f*,0 | 0,0,0 | 0,0,0 | 0,0,0 | *f*,*f*,0 |
| DNS 3 | 0,0,0 | *f*,*f*,*f* | 0,*f*,*f* | 0,*f*,*f* | 0,0,*f* | *f*,*f*,*f* |
| DNS 4 | *f*,0,0 | *f*,*f*,*f* | *f*,*f*,*f* | 0,*f*,*f* | *f*,*f*,*f* | *f*,*f*,*f* |

### 3.3. Second and higher order moments

Figs. 5–7 present the effect of wall permeability on the rms-velocity fluctuations. While the axial and circumferential components are zero at the wall for DNS 1, 2, 3 due to the no-slip constraint, these values are finite for a pipe with openings (DNS 4). Between the wall and the position of maximum TKE production, the turbulence activity is enhanced compared to the solid wall case. In a thin layer of the order of the classical viscous sublayer, the stress-free boundary conditions along with the finite wall normal fluctuations lead to a local maximum of $u_{z,\mathrm{rms}}$ at the 'wall' and to a local maximum of $u_{r,\mathrm{rms}}$ within that layer. Fig. 8 shows the total shear stress and the Reynolds shear stresses for DNS 1, 2, 3, 4. The wall openings generate a non-zero Reynolds shear stress along the wall. Accordingly the viscous stress is reduced there. The flatness

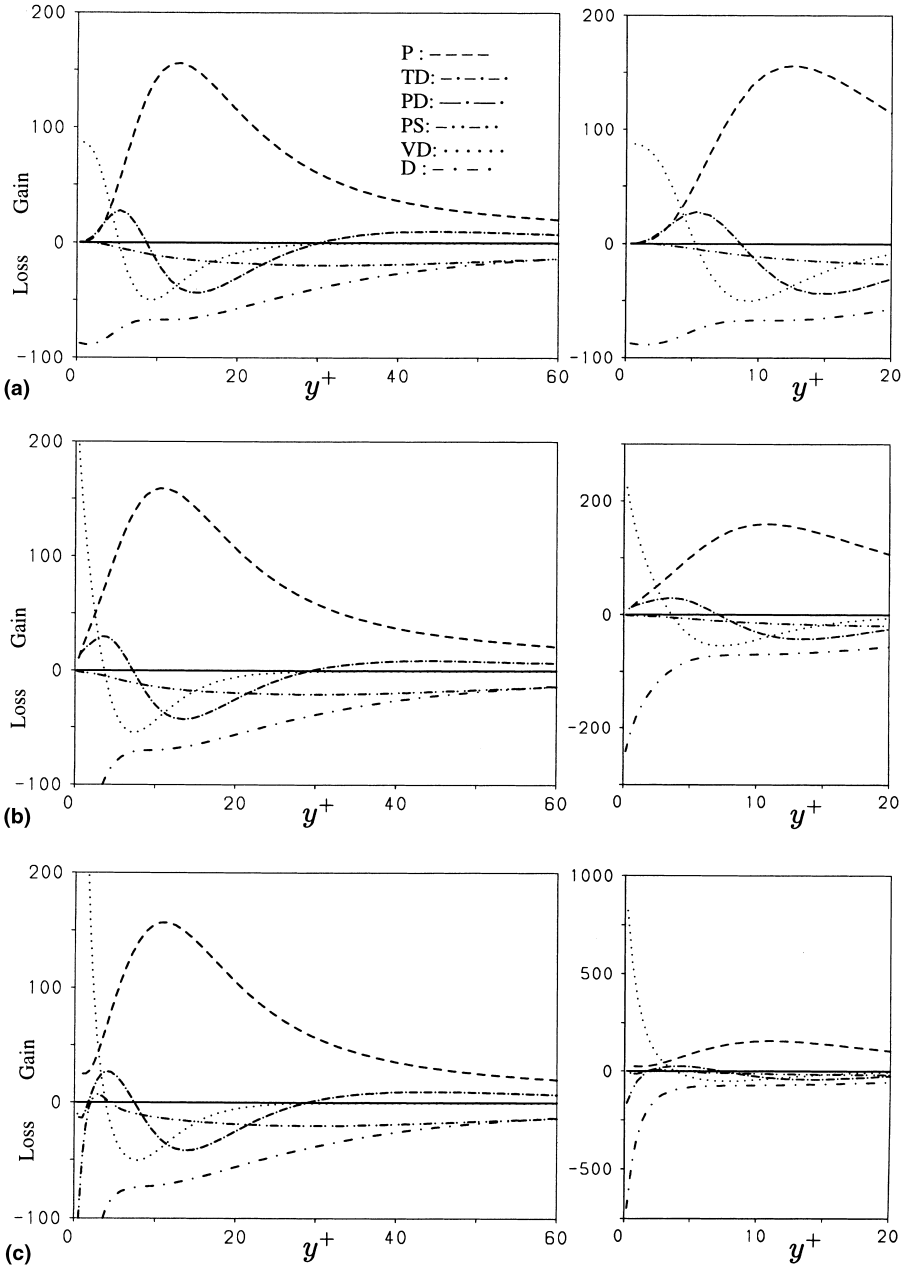


Fig. 13. Terms in the budgets of $\langle u_z'^2\rangle$ for DNS 1 in (a), DNS 3 in (b) and DNS 4 in (c). Lines as in (a).

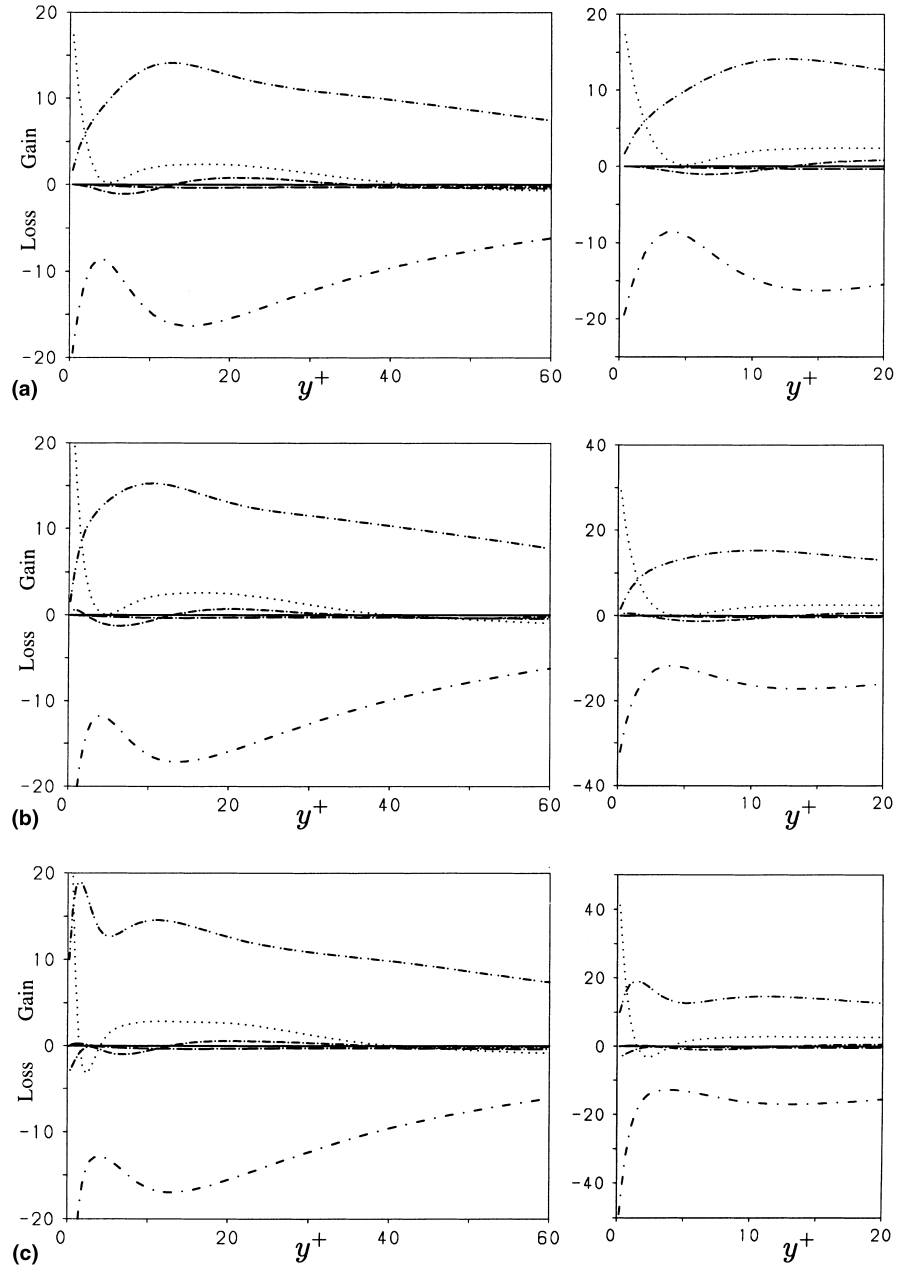


Fig. 14. Terms in the budgets of $\langle u_\varphi'^2 \rangle$ for DNS 1 in (a), DNS 3 in (b) and DNS 4 in (c). Lines as in Fig. 13.

factor of fluctuating quantities indicates intermittency effects when it reaches high values and random motion (a Gaussian p.d.f.) for a value of three. In this sense, the wall normal velocity fluctuations reflect an intermittent behaviour close to a solid wall which, according to Xu et al. (1996), is due to strong sweep events, see Fig. 11. Wall permeability tends to reduce the high near-wall amplitudes of $F(u_r')$ and to increase those of $F(u_z')$ and $F(u_\varphi')$, see Figs. 9–11. The pipe with openings (DNS 4) does not seem to follow the behaviour of the two other permeable pipes (DNS 2,3) what the axial fluctuations are concerned about (Fig. 9).

The fact that $F(u_z')$ has lower values close to the wall than even the solid wall case (DNS 1) is, however, due to the near-wall increase in the axial rms-velocity fluctuations.

Sweeps and ejections generate streaky structures close to the wall as already pointed out. These streaks are commonly visualized plotting contours of the instantaneous axial velocity fluctuations in wall parallel planes (see Fig. 2). In order to demonstrate their statistical relevance, contours of two-point correlations of the axial velocity fluctuations

$$R_{u_z u_z} = \left\langle u_z'(z, \varphi, y^+ = 14) u_z'(z + \Delta z, \varphi + \Delta\varphi, y^+ = 14) \right\rangle, \qquad (17)$$

of DNS 1 and DNS 4 are plotted in Fig. 12 at a wall distance of $y^+ = 14$. From these a mean streak spacing of $\lambda^+ \approx 120$ is deduced in the solid pipe (DNS 1) and of 110 for the wall openings of DNS 4.

### 3.4. Reynolds stress budgets

For a better understanding of the changes in the turbulence structure due to wall permeability, we present profiles of all the

terms appearing in the transport equations for the stresses. The three cases DNS 1, DNS 3 and DNS 4 are compared. The equations for the fully developed, non-swirling flow can be found in Eggels et al. (1994).

The symbols used indicate production (P), turbulent diffusion (TD), pressure-diffusion (PD), pressure-strain (PS), viscous diffusion (VD) and dissipation (D). For better visibility, only parts of the profiles are presented, namely those from the wall up to $y^+ = 60$. Since the near-wall behaviour of the terms strongly depends on their wall values, we provide a table Table 2 showing whether these values are zero (0) or finite ($f$).

Several terms have finite values at permeable walls only due to transverse curvature. This is true for various PS, PD and TD terms and constitutes the differences to corresponding channel flow. In Figs. 13–15, we discuss the effect of wall permeability on the budget of each of the normal stresses, starting with the axial component, Fig. 13. While in solid walls viscous diffusion and turbulent dissipation balance, there is a non-negligible contribution to this balance from the pressure-strain correlation at a wall with openings (DNS 4). Moreover, the amplitudes of VD and D at the wall are strongly increased (DNS 4). This is already the case at walls which allow only for $u_r$-fluctuations (DNS 3). The peak values in the production rates are practically unmodified. The nearly linear increase in P close to the permeable wall of DNS 3 is a consequence of the behaviour of the Reynolds shear stress. The budgets of $\langle u_\varphi'^2 \rangle$ are shown in Fig. 14. This component gets energy from the longitudinal component via redistribution. The PS-term of the $\langle u_\varphi'^2 \rangle$ peaks where the production term of $\langle u_z'^2 \rangle$ has its maximum. The PS-term, however, peaks a second time even closer to the wall in DNS 4. This effect correlates properly with the large negative values of PS in the $\langle u_z'^2 \rangle$-budgets and with the

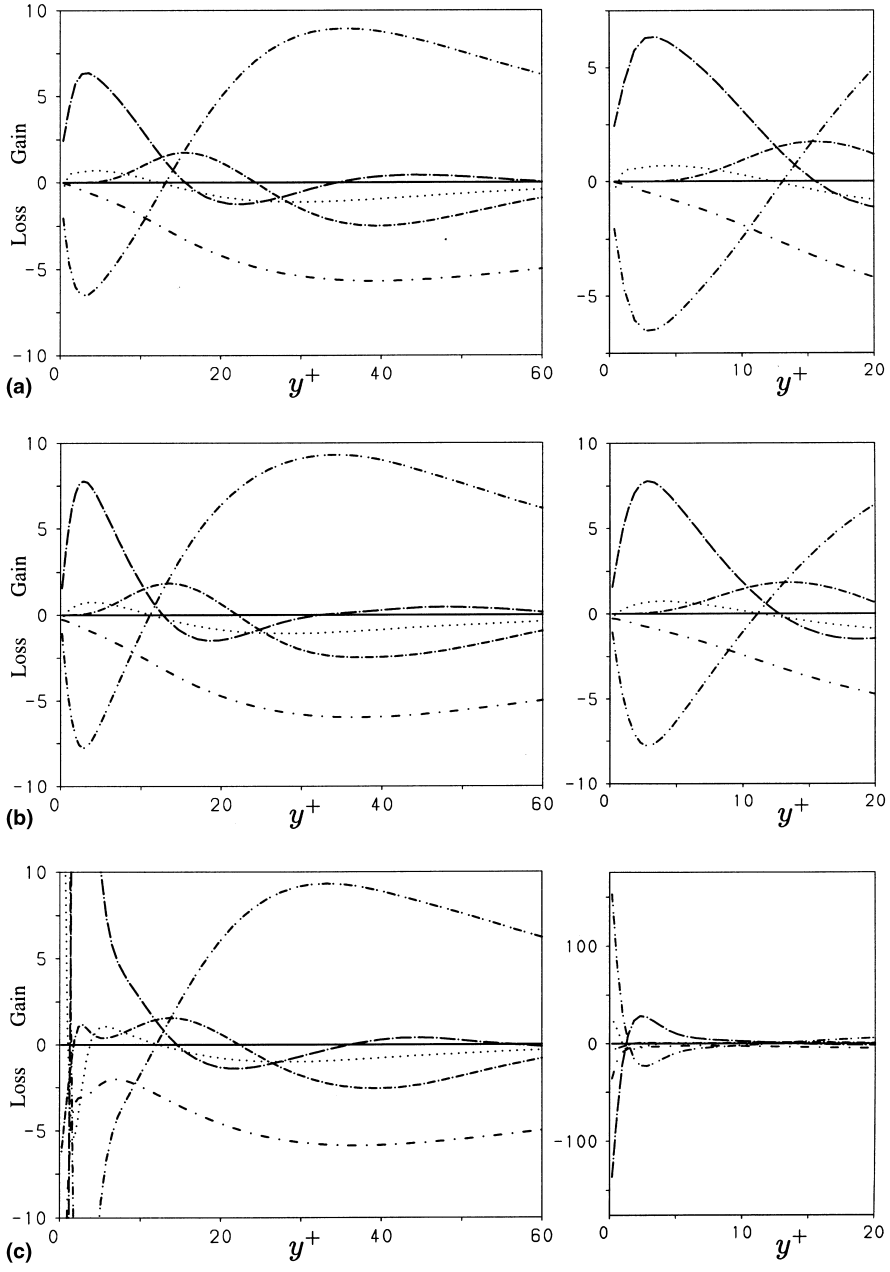


Fig. 15. Terms in the budgets of $\langle u_r'^2 \rangle$ for DNS 1 in (a), DNS 3 in (b) and DNS 4 in (c). Lines as in Fig. 13.

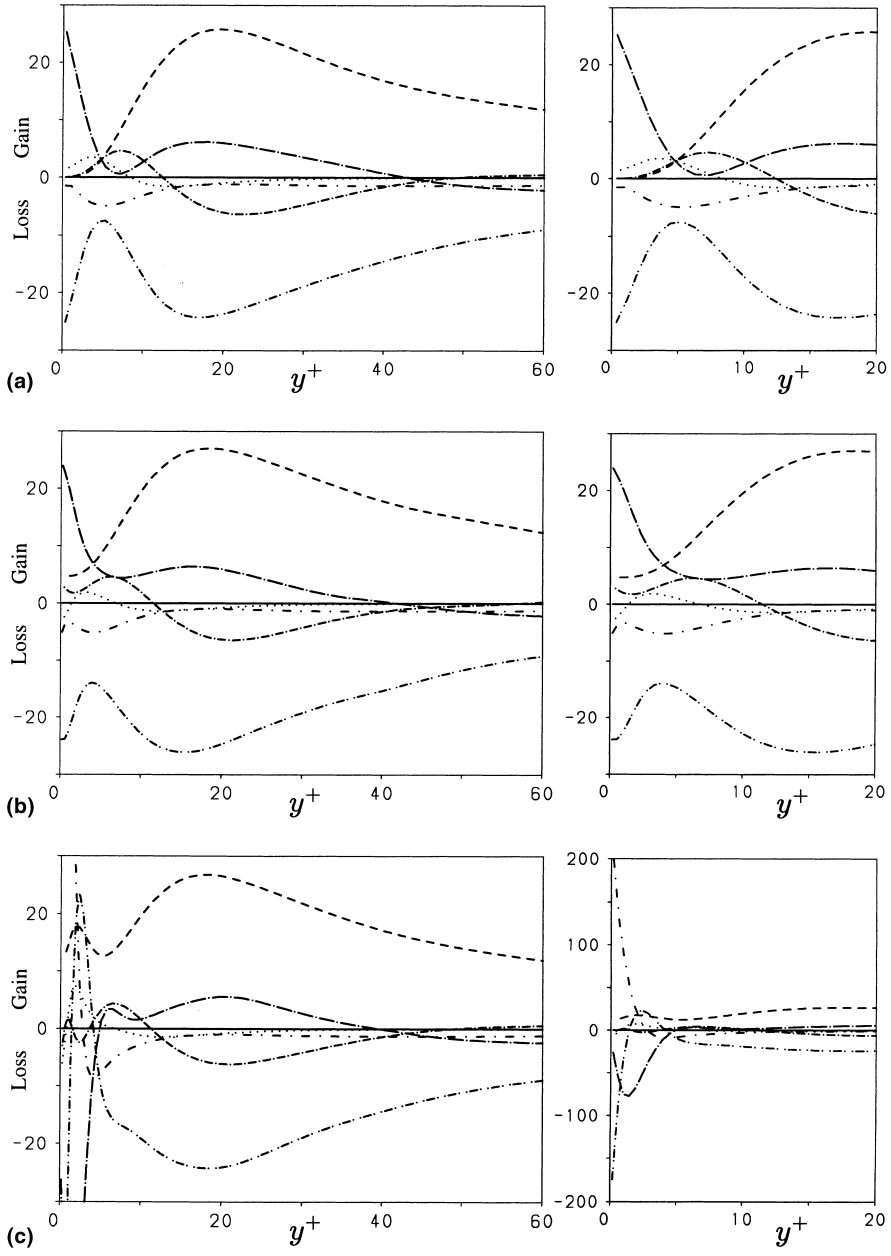


Fig. 16. Terms in the budgets of $\langle u_z' u_r' \rangle$ for DNS 1 in (a), DNS 3 in (b) and DNS 4 in (c). Lines as in Fig. 13.

relative maximum in the axial rms-velocity fluctuations (Fig. 5). The overall behaviour of the other budget terms is quite similar in all the three cases. From the $\langle u_r'^2 \rangle$-budget, it is known (already from channel flow) that PS and PD have peaks and balance within the viscous sublayer of a solid wall. The same balance still holds for DNS 3 and the peaks are even at the same positions. The peak amplitudes have, however, increased by more than 20%. A further increase in these locally maximal amplitudes is observed in case of DNS 4. Yet, PD and PS do not attain zero wall values, but extreme values on the opposite sides. This is probably the most striking feature of this flow case, namely positive PS-values at the wall with openings, which are roughly 16 times larger than those at the peak position of $\langle u_r'^2 \rangle$ in solid pipe flow. It sheds some light on the importance of PS and PD-modelling in the balance equation for the velocity fluctuations in the direction of mean shear of shear driven turbulence.

The $\langle u_z' u_r' \rangle$-budget in Fig. 16 reveals a balance between production ( P) and pressure-strain ( PS) away from the wall for DNS 1, 3 and 4. Close to the wall PS peaks in all cases and is balanced by PD in DNS 1 and DNS 3. The stress-free wall openings of DNS 4 generate high positive dissipation rates at the wall, which balance PS at values exceeding those of DNS 1 and 3 by a factor of 10.

## 4. Conclusions

Direct numerical simulation was used to investigate the changes in the turbulence structure induced by wall permeability which to first order act as wall roughness in fully developed, non-swirling pipe flow. It is found that walls with openings (DNS 4) in which zero-stress conditions are used provide strong changes in the flow structure as compared to

flow in smooth impermeable pipes (DNS 1). These changes are:

- A mean axial slip velocity and a small positive Reynolds shear stress leading to reduced mean viscous stress at the wall, but only slightly reduced bulk velocity.
- Non-zero rms-velocity fluctuations at the wall and in turn enhanced turbulence activity close to the wall.
- The turbulence production rate is non-zero at the wall. Likewise, are pressure-strain and turbulence diffusion terms of the $u_r$-budgets and pressure-diffusion terms of the $(u_\varphi, u_r)$-budgets non-zero.
- The most striking features of DNS 4 are the high positive level of the pressure-strain correlation and the high negative level of the pressure-diffusion term in the $\langle u_r'^2 \rangle$-balance.

These results shed some light on the importance of PS- and PD-modelling especially in the balance equation for the velocity fluctuation in the direction of main shear. It would be interesting to compare these results with detailed measurements in the vicinity of rough walls and to see, to what extent permeable walls are useful models of wall roughness effects.

## References

Eggels, J.G.M., Unger, F., Weiss, M.H., Westerweel, J., Adrian, R.J., Friedrich, R., Nieuwstadt, F.T.M., 1994. Fully developed turbulent pipe flow. A comparison between direct numerical simulation and experiment. J. Fluid Mech. 268, 175–209.

Schlichting, H., 1968. Boundary-Layer Theory, sixth ed., McGraw-Hill, New York.

Wagner, C., Friedrich, R., 1998a. On the turbulence structure in solid and permeable pipes. Int. J. Heat Fluid Flow 19, 459–469.

Wagner, C., Friedrich, R., 1998b. Direct numerical simulation of turbulent flow through permeable or rough pipes. In: Papailiou, K.D. et al. (Eds.), Computational Fluid Dynamics, vol. 1. Wiley, New York, pp. 238–243.

Westerweel, J., Adrian, R.J., Eggels, J.G.M., Nieuwstadt, F.T.M., 1992. Measurements with particle image velocimetry on fully developed turbulent pipe flow at low-Reynolds number. Proceedings of the Sixth International Symposium on Applications of Laser Technique to Fluid Mechanics, Lisbon, Portugal, 20–23 July.

Xu, C., Zhang, Z., den Toonder, J.M.J., Nieuwstadt, F.T.M., 1996. Origin of high kurtosis levels in the viscous sublayer, direct numerical simulation and experiment. Phys. Fluids 8, 1938–1944.